RSC Advances

ROYAL SOCIETY OF CHEMISTRY

www.rsc.org/advances

Tailoring the Adsorption Rate of Porous Chitosan and Chitosan-Carbon Nanotube Core-Shell Beads

An Ouyang,[*ab] Ji Liang[ab]

[a] Department of Mechanical Engineering, Tsinghua University, Beijing 100084, P. R. China

[b] Key Laboratory for Advanced Materials Processing Technology, Ministry of Education, Beijing 100084, P. R. China

*Corresponding author. Email: oyangann@gmail.com.

Abstract

Porous chitosan beads are widely used as adsorption media in environmental and biomedical areas. We present two simple methods to tailor the adsorption behavior of chitosan beads by dynamic adsorption and structural modification. Compressing the chitosan beads repeatedly in solutions containing dye molecules or nanoparticles leads to significant improvement in adsorption rate by enhancing internal molecular diffusion, compared with statically placed beads. We also create a hierarchical core-shell structure consisting of a single-walled carbon nanotube network uniformly wrapped around each chitosan bead, in which the outside nanotube network can block or slow down the diffusion of larger size nanoparticles without influencing adsorption of small size molecules and nanoparticles. Our strategy involving dynamic adsorption and fabrication of hierarchical porous structures might be applied to many other porous materials to tailor their adsorption properties.

Keywords: chitosan beads, porous material, carbon nanotube, core-shell structure, adsorption.

1. Introduction

Chitosan is a natural glucosamine biopolymer and has been fabricated into small porous beads for applications such as environmental adsorption, biomedical immobilization , protein delivery and activation.[1-3] Previous studies have mainly focused on the fabrication methods and the adsorption kinetics for a variety of metal ions and biological molecules.[4-6] For example, different porous structures of chitosan beads have been produced by porogen pore forming, phase inversion method, freeze casting, microfluidic method or by adjusting synthesis parameters.[7-13] The adsorption of various transitional or toxic metal ions by chitosan beads have been investigated based on the surface characteristics and molecular interaction (complexes formation). Those studies were based on a simple and homogeneous bead structure (perhaps with tunable pore sizes), and chemical functionalization was involved to improve molecular adsorption. [14-18] Although their mechanical properties such as the compressive strength were measured, the structural deformability of porous chitosan beads has not been explored in most of applications. [7, 19]

The adsorption rate determines how fast foreign molecules can be attracted to the chitosan beads, and is an important criterion for evaluating the performance of adsorbents. [20, 21] Previously, main methods used to improve the adsorption rates of macroscopic porous adsorbents include grafting functional groups on the bead surface, and introducing other materials such as polymers into the bead to make a composite.[15, 19, 22-25] Those methods focused on surface modification rather than building novel architectures or utilizing the external adsorption conditions. For porous materials with high surface area, it is critical for the molecules or ions to diffuse into the inner part quickly in order to achieve maximum adsorption capacity. For flexible porous materials such as chitosan beads, one of

the potential methods to improve the internal diffusion is to induce structural deformation during adsorption, so that promote liquid transport through the pores. However, mechanical properties of chitosan beads (such as their deformation and elastic recovery under cyclic compression) have not been exploited to improve the adsorption performance. Compared to traditional chemical methods (e.g. grafting functional groups), we explore the structural deformation and modification approaches by making chitosan-carbon nanotube hierarchical porous structures and inducing dynamic adsorption under cyclic compression. Previously, bulk multi-walled carbon nanotube sponges were used to filtrate Au nanoparticles from solution,[26] while here we investigate the adsorption property of chitosan beads and use a single-walled carbon nanotube (SWNT) thin film with much smaller pores than the bead surface openings to tailor the adsorption behavior for nanoparticles with different sizes.

Here, we show that the adsorption rate of chitosan beads can be tailored by simple methods such as dynamic adsorption and structural modification. We performed dynamic adsorption by repeatedly compressing the chitosan beads in situ during adsorption, which significantly improved the adsorption rate compared with static condition (without compression). Also, we constructed a hierarchical core-shell structure by wrapping a thin film of SWNTs on the chitosan beads, so that applied a porous nanotube membrane on the bead surface. This core-shell structure allows infiltration of dye molecules and small size nanoparticles, but blocks larger size nanoparticles, resulting in lower adsorption rate compared with bare chitosan beads. Related mechanisms such as the compression behavior of chitosan beads and the interaction between nanotubes and nanoparticles have been analyzed.

2. Results and Discussion

2.1 Chitosan beads and mechanical properties

The spherical chitosan beads with diameters of 2-2.5 mm were fabricated by freeze casting of a chitosan solution mixed with multi-walled carbon nanotubes, which were dropped in liquid nitrogen (See Experimental). The nanotubes were added into the chitosan matrix to improve the porous structure as absorbent. The entire bead is an open-porous structure, and from the surface we can see macropores and channels made by chitosan skeletons with dendritic lamellar morphology running along the ice crystallization direction, a unique feature of the freeze-casting product with water (Fig. 1a). The pore sizes on the surface are in the range of 5 to 15 μm which allow diffusion and transportation of outside molecules into the inside (Fig. 1b).

These porous chitosan beads are compliant and can recover to original shape after deformation. We have tested the mechanical properties by compressing a single bead to predefined strains in dry (in air) or wet states (immersed in water) (as illustrated in Fig. 1c). Load-strain curves for compressive strains from 10% to 50% in air show increasing strength at higher strain, and complete or partial recovery during unloading (Fig. 1d). The compressive stress is about 0.4 MPa at ε=50% estimated from a bead diameter of 2 mm, but the stress is changing during compression because of the spherical shape. Within a moderate strain (ε=20%), the bead shows elastic recovery at the beginning and develops a small residual strain after 100 compression cycles (Fig. 1e). Plastic deformation becomes more severe when the bead is compressed to higher strain, for example, the residual strain is about 21% after 1 cycle compression to ε=50% (Fig. 1f). However, the bead shows enhanced elasticity when it is immersed in water, and plastic deformation disappears after compression. This is due to the adsorption of water during the unloading process that helps the bead to simultaneously expand and recover to original shape. Elastic recovery of chitosan beads is a favorable property for dynamic adsorption by deforming the beads in solution, as discussed later.

2.2 Adsorption of dye molecules under dynamic or static conditions

We first tested the adsorption properties of chitosan beads placed in a solution of methyl orange (MO) in water (0.02 mM). Dynamic adsorption was enabled by manually compressing each bead one time every 15 minutes. We used a tweezer to squeeze the bead in the solution, and the bead recovered quickly to spherical shape after releasing. This compression process facilitated molecular diffusion into the inner pores of chitosan beads by uptaking and extruding the solution from the beads repeatedly. For static condition, the beads were simply placed in the solution without being deformed. As a result, the MO adsorption under dynamic condition is much faster than static condition. We used UV-Vis spectroscopy to monitor the dye concentration during the adsorption process, and the spectra after every 1 hour were summarized in Fig. 2a for both conditions. The peak intensity at 464 nm (characteristic peak of MO) decreases over the period consistently, indicating continuous adsorption of MO and decrease of the solution concentration. Based on the initial solution concentration (0.02 mM) and the change of optical absorption peak intensity after certain time, we have plotted the adsorption capacity versus time curves for the chitosan beads under static and dynamic conditions, respectively (Fig. 2b). The dynamic condition results in much higher adsorption rate (0.024 $mg \cdot g^{-1} \cdot min^{-1}$ at the beginning stage) and adsorption capacity for MO (e.g. 3.09 $mg \cdot g^{-1}$ at 240 min) than the adsorption rate (0.014 $mg \cdot g^{-1} \cdot min^{-1}$) and capacity (1.86 $mg \cdot g^{-1}$ at 240 min) measured under static condition. The mechanical flexibility and elasticity of chitosan beads are important factors to sustain structural deformation for dynamic adsorption, which result in enhanced adsorption capacity and rate.

2.3 Surface modification and core-shell chitosan-SWNT structures

Next, we show that the structure of chitosan beads can be modified to tailor the adsorption

property. Previously, we have synthesized spiderweb-like, freestanding SWNT films consisting of interconnected SWNT bundles by chemical vapor deposition (CVD).[27] Here, a freestanding SWNT film was cut into appropriate size to wrap individual chitosan beads to form core-shell structures by a solution transfer process and freezing drying (Fig. 3a,3b). Scanning electron microscopy (SEM) characterization shows that the chitosan-SWNT bead remains a spherical shape (Fig. 3c). Enlarged view shows that the SWNT film covers the bead surface uniformly (Fig. 3d). We find that a SWNT film is suspended on the initially open pores and channels at the bead surface, and the underlying chitosan walls can be seen through the SWNT film (Fig. 3e). Further SEM characterization reveals that the SWNT film is seamlessly attached to the chitosan bead surface, forming a well-adhered contact area (Fig. 3f, 3g). Since the SWNT network has much smaller pores (tens to hundreds of nm) than the chitosan pores (several μm), we obtain a hierarchical structure with different pore distribution at the surface (SWNT) and core part (chitosan). This is a very thin (single-layer), porous SWNT membrane attached to the chitosan bead as an outer shell. Because surface pores are the only channel provided for molecules to enter the chitosan beads, our structural modification might influence the adsorption properties due to the presence of an outer SWNT membrane, intersecting the molecular transport path.

We have also carried out transmission electron microscopy (TEM), Raman, Attenuated Total Reflectance-Fourier Transform Infrared spectroscopy (ATR-FTIR) and Brunauer-Emmett-Teller (BET) specific surface area test to further characterize the structure of the chitosan beads and the SWNT film. First, TEM image shows that the SWNT film consists of interconnected single-walled nanotubes and small bundles (Fig. S2a). Raman spectrum also reveals many radial breathing mode peaks of the SWNTs, indicating the presence of different diameter nanotubes (Fig. S2b). The specific

surface areas of the chitosan and chitosan-SWNT beads calculated from their nitrogen adsorption-desorption isotherms at 77 K using BET method are about 26 and 64 m^2/g, respectively (Fig. S2c, S2d). The core-shell chitosan-SWNT beads show enhanced specific surface area and also an increased pore volume in the range of 10-100 nm (coming from SWNTs) than chitosan beads. FTIR spectra of the chitosan and chitosan-SWNT beads show chitosan-related peaks in both samples, including C-O stretching vibrations (1065, 1024 cm^{-1}), amide II bands (1547, 1554 cm^{-1}), and C-H stretching vibrations (2872, 2852 cm^{-1}) (Fig. S2e). There are also an O-H (3363 cm^{-1}) and C=O (1732 cm^{-1}) stretching vibration peaks appearing in both beads, which may come from the chitosan bead (containing multi-walled nanotubes) and the SWNTs. The SWNT shell does not add new functional groups to the chitosan bead.

2.4 Molecular and nanoparticle adsorption by chitosan and chitosan-SWNT beads

For the above two structures, chitosan and chitosan-SWNT core-shell beads, we compared their adsorption properties of dye molecules and nanoparticles with relatively small or large sizes. We adopted dynamic conditions for both samples (compressing beads in the solution cyclically during the process). The adsorption process in the MO solution can be monitored by UV-Vis spectra, in which the peak intensity at 465 nm decreases continuously over time. The spectra measured from the solutions containing equal weight chitosan or chitosan-SWNT beads with the same initial concentration (0.02 mM) and after the same period (e.g. 0.5, 1 hour) are very close, indicating similar adsorption rates by these two samples (Fig. 4a, 4b). The dropping of MO concentration (peak intensity) is comparable for both samples until equilibrium, indicating that the SWNT membrane does not block the infiltration of dye molecules into the beads.

We also tested the adsorption of Au nanoparticles with different diameters (5 and 50 nm,

respectively) synthesized by a solution method as described early [26] to study the effect of nanoparticle size. For 5 nm Au nanoparticles, the chitosan and chitosan-SWNT beads show similar adsorption rates during a period of 50 hours, according to the recorded UV-vis spectra in which the characteristic peak at 520 nm nearly vanishes at the end (Fig. 4c, 4d). However, for 50 nm Au nanoparticles, we see clear difference between the two samples. The peak intensity at 537 nm recorded in the solution containing chitosan beads drops faster than the solution containing chitosan-SWNT beads, indicating the former has a higher adsorption rate for 50 nm Au nanoparticles (Fig. 4e, 4f). Both chitosan and chitosan-SWNT beads show similar adsorption capacities for MO (2.75 and 2.81 $mg \cdot g^{-1}$ at 240 min, respectively) and 5 nm Au nanoparticles (both are 5.76 $mg \cdot g^{-1}$ at 3000 min). However, for 50 nm Au nanoparticles, chitosan-SWNT beads show a lower adsorption capacity (4.67 $mg \cdot g^{-1}$ at 240 min) than the chitosan beads (5.92 $mg \cdot g^{-1}$ at 240 min). Correspondingly, the adsorption rate of the former (0.091 $mg \cdot g^{-1} \cdot min^{-1}$) was slightly lower than the latter (0.121 $mg \cdot g^{-1} \cdot min^{-1}$) during the first 30 min. It also implies that the SWNT membrane at the bead surface could influence (slow down) the adsorption of nanoparticles if the particle size is sufficiently large.

We have characterized the surface morphology of core-shell chitosan-SWNT beads after adsorption of different size Au nanoparticles. SEM images in Figure 5 show two beads after adsorbing 5 nm and 50 nm Au nanoparticles for the same time (240 min), respectively. It can be clearly seen that the size of 5 nm nanoparticles is much smaller than the pore sizes (on the order of 1 μm or less) of the SWNT network, therefore most of them can smoothly pass through the network and reach the chitosan bead to be adsorbed (Fig. 5a, 5b). At the same time, a small amount of the 5 nm nanoparticles have been adsorbed by the SWNT bundles, particularly at the crossed positions of SWNTs and thick bundles (Fig. 5b, 5c). In comparison, there are many 50 nm Au nanoparticles

distributed throughout the SWNT network (Fig. 5d, 5e), which either attached individually to interconnected bundles or form small aggregations within the network pores (Fig. 5e, 5f). We also have characterized chitosan beads (without a SWNT shell) after adsorption of 50 nm Au nanoparticles, and observe uniformly adsorbed nanoparticles on the pore walls inside the bead (Fig. S2), indicating that the chitosan has a strong adsorption to Au nanoparticles.

The adsorption process by core-shell chitosan-SWNT beads includes two sequential steps. The first step is that the SWNT film (shell) adsorbs the molecules and particles coming from the solution, and simultaneously provides many porous channels for diffusion. The second step is the adsorption of diffused species by the inner chitosan bead (core). The core and shell have different roles. The chitosan beads have a bulk three-dimensional highly porous structure, and act as the main body for adsorption. The thin SWNT film acts as a porous network for particle diffusion and also may adsorb some particles as well as block large size particles. During adsorption, smaller size molecules and nanoparticles can easily penetrate through the SWNT network and enter the chitosan bead. High resolution TEM characterization reveals very less 5 nm Au nanoparticles adhered on the SWNT bundles (Fig. 5c). Therefore, for MO and 5 nm Au nanoparticles, the adsorption by the chitosan bead plays a dominating role, and its total capacity is similar to that of the chitosan beads without SWNT films (Fig. 4b, 4d). In contrast, we observe many larger size nanoparticles intersected by the SWNT network. As the adsorption process continues, more 50 nm Au nanoparticles accumulated on the SWNT film and blocked some of the pores, which could slow down the diffusion and reduce the adsorption capacity by the chitosan beads. Therefore for core-shell chitosan-SWNT beads, both the core and shell adsorption occur and contribute to the total adsorption capacity. The presence of a SWNT film could influence the adsorption process of chitosan bead, especially for larger size

nanoparticles.

3. Conclusions

We demonstrated two methods to tailor the adsorption behavior of porous chitosan beads, by dynamic adsorption (compressing beads) and structural modification (covering a SWNT membrane on the bead surface). Our hierarchical chitosan-SWNT core-shell structure has different pore distributions at the surface (SWNT film) and inside (chitosan bead), which can influence the adsorption property. The SWNT membrane at the bead surface could block nanoparticles with certain size, and may be used for selective filtration and transport through the chitosan pores. Chemical functionalization on the core-shell beads, or controlling the thickness and pore morphology of the SWNT films could further improve the adsorption performance and selectivity. The methods and materials presented here have potential applications in selective adsorption, drug delivery, and environmental cleanup.

Acknowledgment.

We thank Anyuan Cao, Yuanyuan Shang, Enzheng Shi and Yanbing Yang in Peking University for help in mechanical testing and discussions.

4. Experimental

4.1Materials

The chitosan (degree of deacetylation=80%~95%) and methyl orange were purchased from Sinopharm Chemical Reagent Co., Ltd. Multi-walled carbon nanotubes were provided by CNano Technology Limited. and were treated by both nitric acid (65%-68%, v/v, A.R. Beijing Chemical Works) and sulfuric acid (95%-98%, v/v, A.R. Beijing Chemical Works) (1:3 volume ratio), boiling under a reflux condenser for 30min. The SWNT thin film was fabricated by a floating catalyst CVD method in a horizontal furnace. A mixed solution of xylenes (carbon source), ferrocene (catalyst precursor) and a small amount of sulfur was injected into the furnace by an automatic syringe pump at a feeding rate of 2-4 μL min^{-1}, and carried by a gas mixture of Ar (2500 sccm) and H_2 (600 sccm) to the reaction zone. The reaction temperature was set to 1150-1170°C for growing freestanding SWNT films. The specific surface area of the SWNT film is 150-250 m^2/g. Glacial acetic acid (A.R. Beijing Chemical Works) was used to dissolve the chitosan. Au nanoparticles with different sizes (5 nm and 50 nm in diameter, respectively) were synthesized by reduction of $HAuCl_4$ under different conditions [25] to prepare aqueous solutions for adsorption experiments.

4.2 Preparation of chitosan beads and core-shell chitosan beads

Chitosan powders were dissolved by 1% (in volume) acetic acid and mixed with multi-walled carbon nanotube aqueous solution at a weight ratio of 3:2, and stirred at 60°C until complete dissolution. After that, the mixed solution was injected through a syringe needle (0.7 mm diameter) and dripped onto liquid nitrogen drop by drop to make frozen beads. Samples were freeze-dried for 24 h and had a diameter range of 2 to 2.5 mm. The resulting porous chitosan beads contain 40 wt% multi-walled nanotubes which were uniformly embedded within the chitosan matrix and reinforced the chitosan framework. A SWNT film was cut into an appropriate size (e.g. about 8×15 mm in square shape), floated on water surface in the petri dish, and then a chitosan bead was immersed underneath to pick up the film. This SWNT film size could ensure overall wrapping of a 2.5 mm diameter chitosan bead without much overlapping or forming multi-layer shells. The SWNT film wrapped the chitosan bead tightly after freeze drying, forming a core-shell chitosan-SWNT bead with a hierarchical porous structure.

4.3 Adsorption of MO and Au nanoparticles under dynamic or static conditions

MO was dissolved in deionized water at a concentration of 0.02 mM. Colloids containing 50 nm Au nanoparticles or 5 nm Au nanoparticles were synthesized separately at concentrations of 0.1 mM and 0.66 mM for adsorption tests.

A 20 mg sample of the synthesized chitosan beads was added to 10 mL of 0.02 mM MO solution for two petri dishes with the same solid to liquid ratio. Dynamic adsorption was enabled by manually compressing each bead one time every 15 minutes using a tweezer, while in static adsorption the beads were simply placed in the solution without being compressed. For MO and Au nanoparticles adsorption tests, we used the same weight of chitosan and chitosan-SWNT beads (20 mg, about 10-15 beads) and tested in dynamic conditions.

After adsorption, the concentration of MO or Au nanoparticles could be analyzed by Cary 5000 and the adsorption capacities were calculated as follows:

$$Q_A = \left(\frac{V(C_0 - C_t)}{m}\right) mg \cdot g^{-1}$$

Where Q_A was the MO or Au nanoparticles' adsorption capacities ($mg \cdot g^{-1}$), C_0 and C_t (mg/L) were the concentrations of MO or Au nanoparticles before and after adsorption in dynamic conditions. V (ml) was the volume of the solution and W (g) was the weight of the adsorbent.

4.4 Mechanical test and characterization

The mechanical test was carried out in a single column material testing instrument (Instron 5843) with a 10 N load cell. The chitosan bead samples selected for testing had a uniform diameter of 2 mm. A single bead was placed on the bottom stage while the top stage moved down to compress the sample at predefined strains (10%-50%) and the compression rate was set as 0.5 mm/min. The cyclic test was performed by compressing the sample repeatedly for 100 times. To test the behavior under water, the bead was immersed in water to allow water adsorption and extrusion during compression cycles. The morphology and structure of the chitosan and chitosan-SWNT beads were characterized by LEO-1530 field emission scanning electron microscope (Germany LEO Company) and transmission electron microscope (FEI Tecnai G2 T20). Raman spectrum was obtained using Raman spectrometer (Renishaw inVia plus), and Attenuated Total Reflectance-Fourier Transform Infrared (ATR-FTIR) spectra were obtained using Nicolet 6700FTIR. The nitrogen adsorption-desorption isotherms of chitosan and chitosan-SWNT beads at 77 K from NOVA4000 were used to calculated the specific surface area and pore size distribution using BET and Barrett-Joyner-Halen (BJH) methods. To monitor the concentration change in MO and Au solutions, UV-vis spectra in the wavelength range of 350 to 800 nm were carried out by Cary 5000 (Agilent Company).

References

[1] Mi FL, Shyu SS, Chen CT, Schoung JY. Porous chitosan microsphere for controlling the antigen release of Newcastle disease vaccine: preparation of antigen-adsorbed microsphere and in vitro release. *Biomaterials*. 1999, *20*(17): 1603-1612.

[2] Li F, Du P, Chen W, Zhang S. Preparation of silica-supported porous sorbent for heavy metal ions removal in wastewater treatment by organic-inorganic hybridization combined with sucrose and polyethylene glycol imprinting. *Anal Chim Acta*. 2007, *585*(2): 211-218.

[3] Mi FL, Shyu SS, Chen CT, Lai JY. Adsorption of indomethacin onto chemically modified chitosan beads. *Polymer*. 2002, *43*(3): 757-765.

[4] Tang H, Zhou W, Lu A, Zhang L. Characterization of new sorbent constructed from Fe_3O_4/chitin magnetic beads for the dynamic adsorption of Cd^{2+} ions. *J Mater Sci*. 2014, *49*(1): 123-133.

[5] Yong SK, Bolan N, Lombi E, Skinner W. Synthesis and characterization of thiolated chitosan beads for removal of Cu(II) and Cd(II) from wastewater. *Water Air Soil Poll*. 2013, *224*, 1720-1732.

[6] Fu GQ, Li HY, Yu HF, Liu L, Yuan Z, He BL. Synthesis and lipoprotein sorption properties of porous chitosan beads grafted with poly(acrylic acid). *React & Funct Polym*. 2006, *66*(2): 239-246.

[7] Zhao H, Xu J, Lan W, Wang T, Luo G.. Microfluidic production of porous chitosan/silica hybrid microspheres and its Cu(II) adsorption performance. *Chem Eng J*. 2013, *229*, 82-89.

[8] Xu J, Xu X, Zhao H, Luo G. Microfluidic preparation of chitosan microspheres with enhanced adsorption performance of copper(II). *Sensor Actuat B-Chem*. 2013, *183*, 201-210.

[9] Fang GZ, Tan J, Yan XP. An ion-imprinted functionalized silica gel sorbent prepared by a surface imprinting technique combined with a sol-gel process for selective solid-phase extraction of cadmium (II). *Anal. Chem*. 2005, *77*, 1734-1739.

[10] Zeng XF, Eli R. Cross-linked macroporous chitosan anion-exchange membranes for protein separations. *J Membrane Sci.* 1998, *148*(2): 195-205.

[11] Catheline A. L. C, Richard A. C, Nadia G, James A.C, Stefan A. F. B. Conducting nanocomposite polymer foams from ice-crystal-templated assembly of mixtures of colloids. *Adv. Mater*. 2009, *21*, 2894-2898.

[12] Etienne M, Eduardo S, Antoni P. T. Architectural control of freeze-cast ceramics through additives and templating. *J.Am. Ceram. Soc.* 2009, *92*(7): 1534-1539.

[13] Sylvain D. Freeze-casting of porous biomaterials: structure, properties and opportunities. *Mater*. 2010, *3*, 1913-1927.

[14] Atia AA, Donia AM, Elwakeel KZ. Selective separation of mercury(II) using a synthetic resin containing amine and mercaptan as chelating groups. *React Funct Polym*. 2005, *65*(3): 267-75.

[15] Shi QH, Tian Y, Dong XY, Bai S, Sun Y. Chitosan-coated silica beads as immobilized metal affinity support for protein adsorption. *Biochem Eng J*. 2003, *16*(3): 317-22.

[16] Hasan S, Krishnaiah A, Ghosh TK, Viswanath DS, Boddu VM, Smith ED. Adsorption of divalent cadmium (Cd(II)) from aqueous solutions onto chitosan-coated perlite beads. *Ind Eng Chem Res*. 2006, *45*(14): 5066-5077.

[17] Xiao Y, Zhou XH. Synthesis and properties of a novel crosslinked chitosan resin modified by L-lysine. *React & Funct Polym*. 2008, *68*(8): 1281-1289.

[18] Wang X, Kong W, Xie W, Li L, Liu Y, Wu X, et al. Bi-porous bioinspired chitosan foams with layered structure and their adsorption for xylenol orange. *Chem Eng J*. 2012, *197*, 509-516.

[19] Liu T, Yang X, Wang Z, Yan X. Enhanced chitosan beads-supported Fe-0-nanoparticles for removal of heavy metals from electroplating wastewater in permeable reactive barriers. *Water Res.* 2013, *47*(17): 6691-6700.

[20] Kawamura Y, Yoshida H, Asai S, Tanibe H. Breakthrough curve for adsorption of mercury(II) on polyaminated highly porous chitosan beads. *Water Sci Technol.* 1997, *35*(7): 97-105.

[21] Ruiz M, Sastre A, Guibal E. Pd and Pt recovery using chitosan gel beads. I. influence of the drying process on diffusion properties. *Sep Sci Technol.* 2002, *37*(9): 2143-2166.

[22] Jiang X, Sun Y, Liu L, Wang S, Tian X. Adsorption of CI Reactive Blue 19 from aqueous solutions by porous particles of the grafted chitosan. *Chem Eng J*. 2014, *235*, 151-157.

[23] Moscofian A. S. O, Pires C. T. G.. V, Vieira A. P, Airoldi C. Removal of reactive dyes using organofunctionalized mesoporous silicas. *J Porous Mat.* 2013, *20*(5): 1179-1188.

[24] Uzun I, Guzel F. Rate studies on the adsorption of some dyestuffs and p-nitrophenol by chitosan and monocarboxymethylated(mcm)-chitosan from aqueous solution. *J Hazard Mater.* 2005, *118*(1-3): 141-54.

[25] Inukai Y, Tanaka Y, Matsuda T, Mihara N, Yamada K, Nambu N, et al. Removal of boron(III) by N-methylglucamine-type cellulose derivatives with higher adsorption rate. *Anal Chim Acta.* 2004, *511*(2): 261-5.

[26] Li H, Gui X, Zhang L, Ji C, Zhang Y, Sun P, et al. Enhanced Transport of Nanoparticles Across a Porous Nanotube Sponge. *Adv Funct Mater*. 2011, *21*(18): 3439-3445.

[27] Li Z, Jia Y, Wei J, Wang K, Shu Q, Gui X, et al. Large area, highly transparent carbon nanotube spiderwebs for energy harvesting. *J Mater Chem*. 2010, *20*(34): 7236-7240.

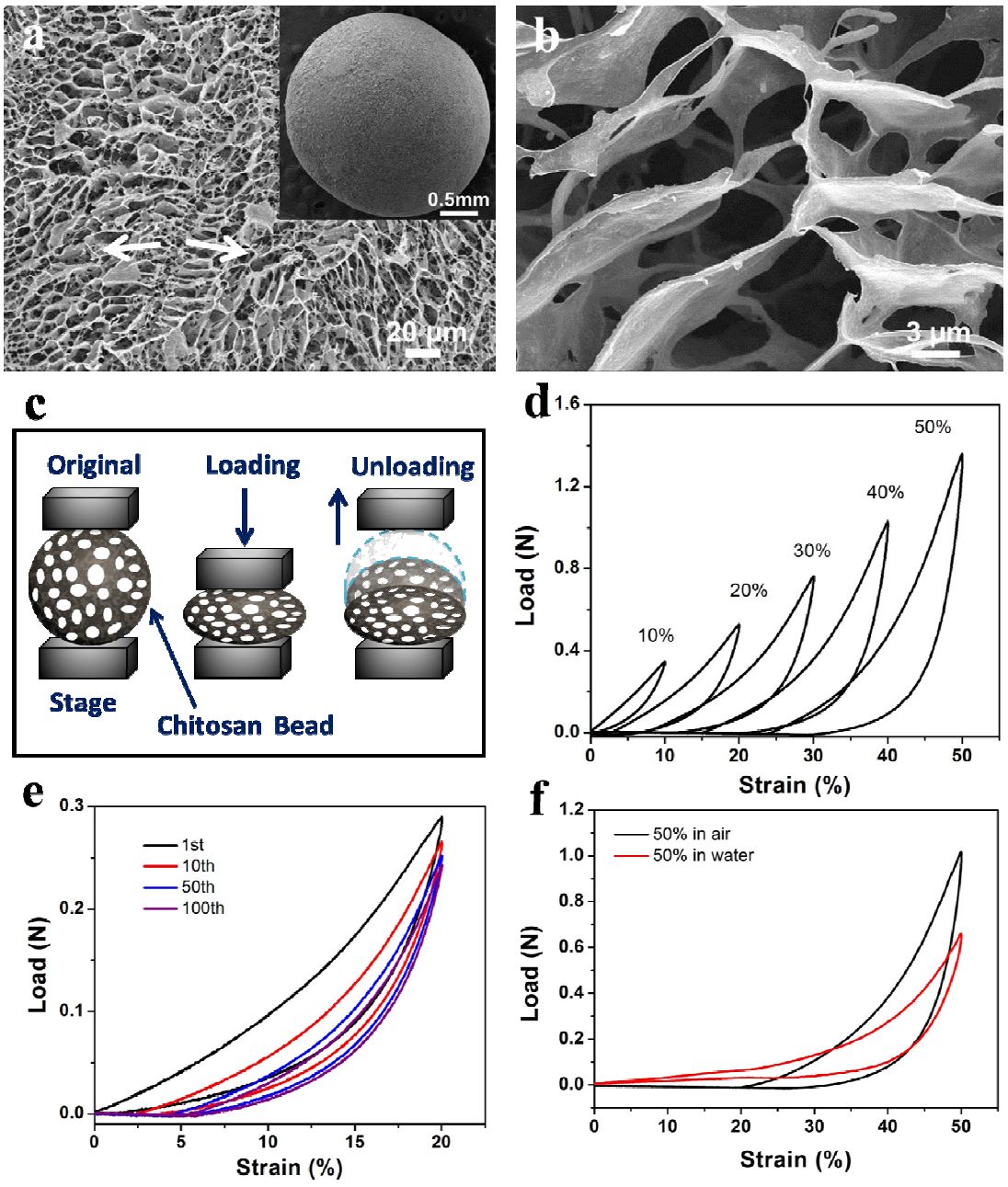

Figure 1. Morphology and mechanical properties of chitosan beads. a) SEM image of the chitosan beads surface, in which the arrows show the direction of dendritic branches; Inset, the entire bead. b) Detailed texture and pore structure on the bead surface. c) Illustration of the dynamic process by compressing chitosan beads cyclically. d) Load-strain curves for predefined compressive strains from 10% to 50% in air. e) Load-strain curves for cycle 1st, 10th, 50th and 100th with a set strain of 20% in air. f) Load-strain curves of compression tests in air and in water to ε=50%, respectively.

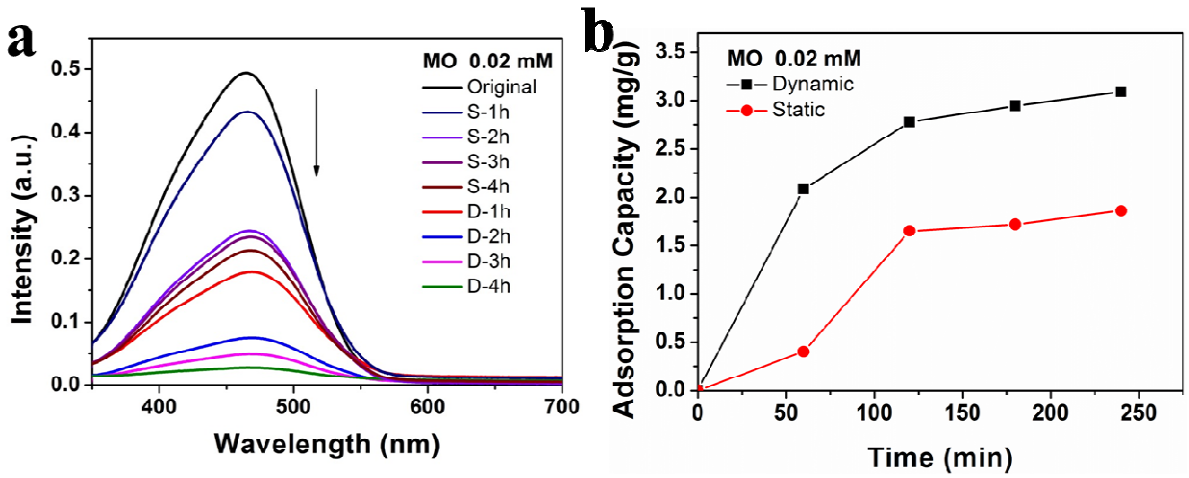

Figure 2. Spectroscopy study for MO adsorption of chitosan beads under dynamic and static conditions. a) UV-vis absorption spectra of the MO solution after different adsorption periods under dynamic and static conditions. S represents static condition and D represents dynamic condition. b) Adsorption capacities of MO by chitosan beads in static and dynamic conditions for a period of 240 min.

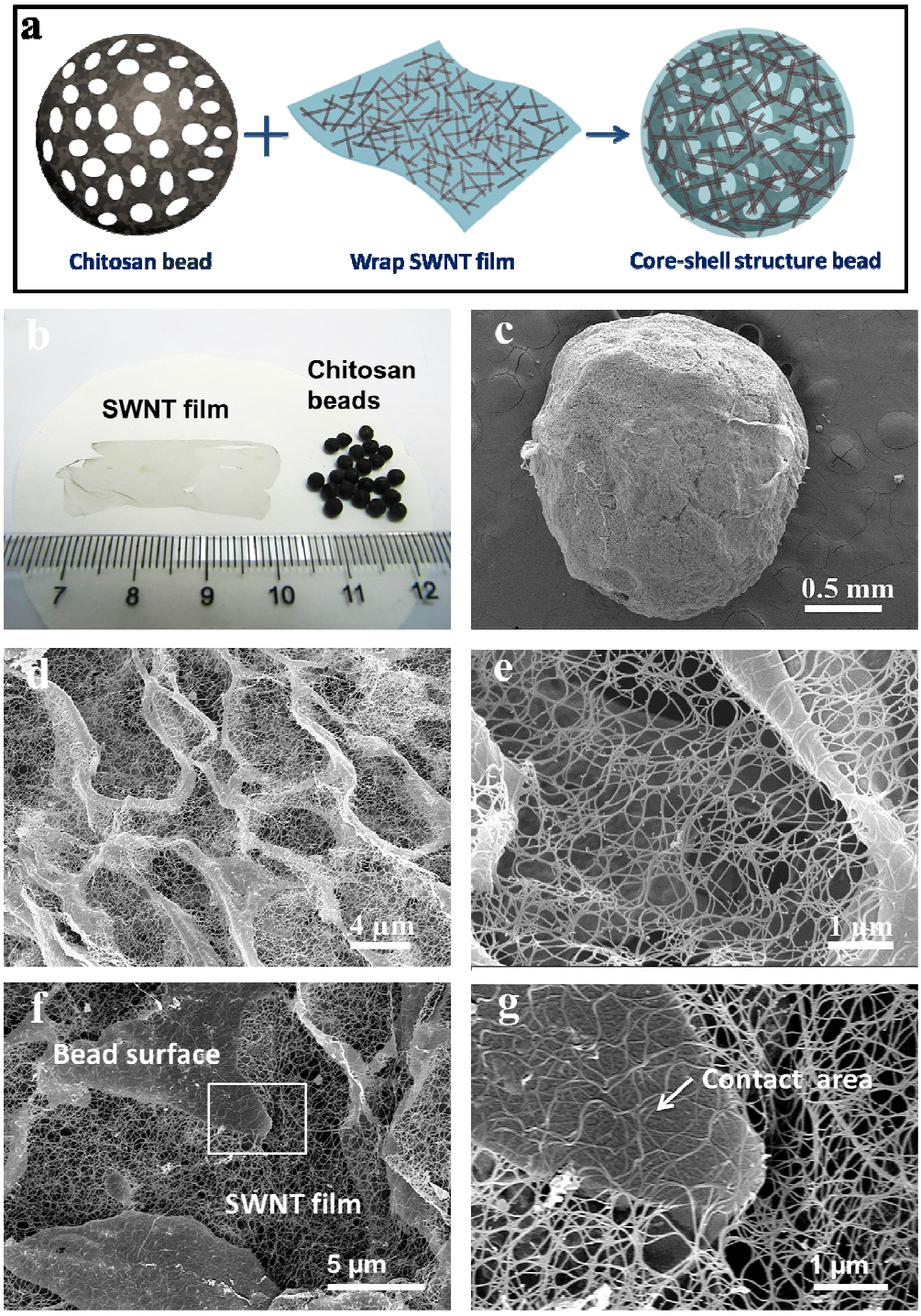

Figure 3. Fabrication and characterization of core-shell chitosan-SWNT beads. a).Schematic for preparation of chitosan-SWNT beads by wrapping a SWNT film onto a chitosan bead. b) Photo of chitosan beads and a SWNT film. c) SEM image of a chitosan-SWNT bead. d) SEM image of the bead surface showing a conformal and uniform coating of SWNT film. e) Detailed view showing the SWNT membrane suspended over the pores. f) SEM image showing seamless attachment of the SWNT film to the bead surface. g) Close view of the contact area showing well adhesion of SWNTs to the underlying bead.

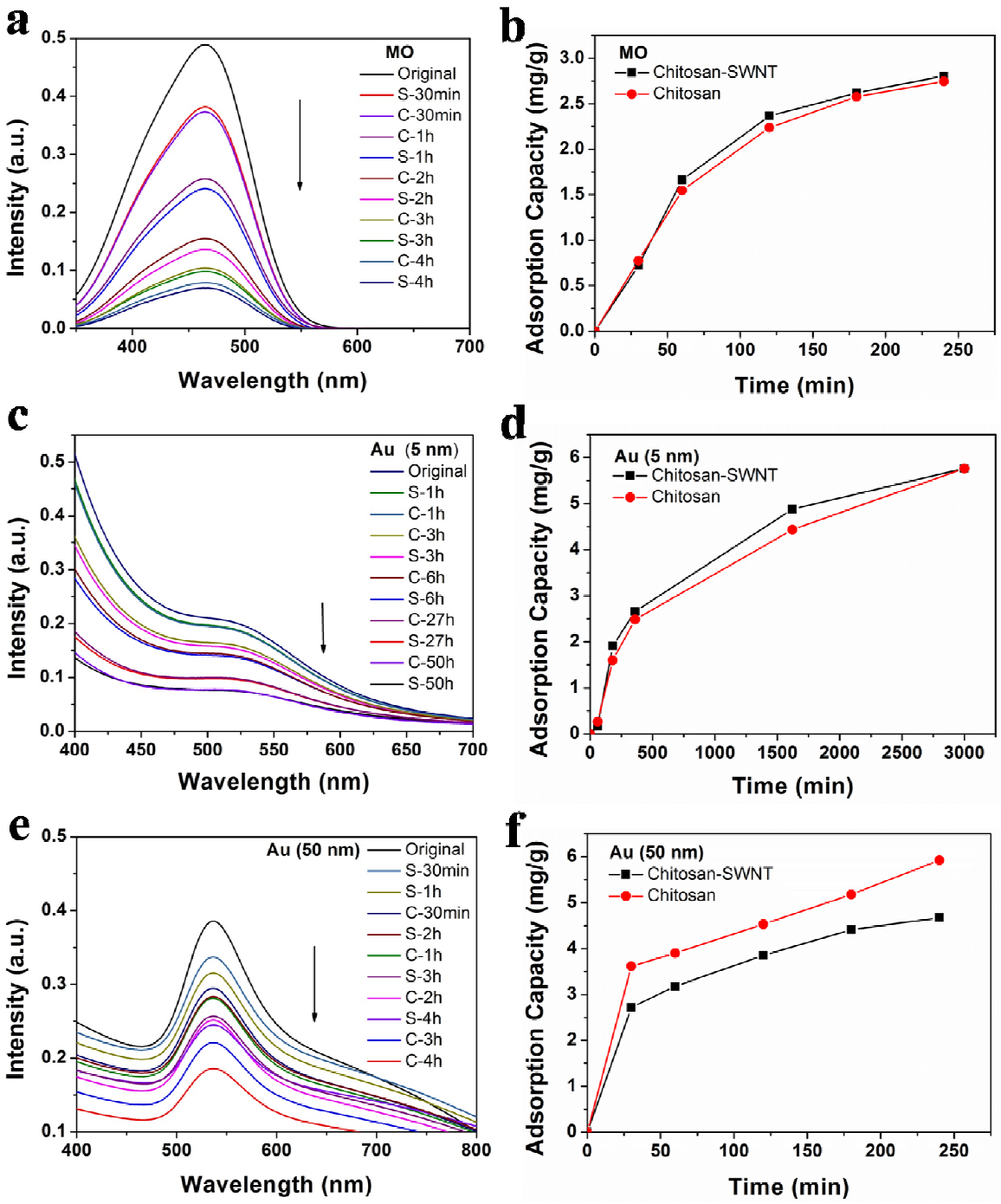

Figure 4. Spectroscopy study on MO and Au nanoparticle adsorption by chitosan (C) and chitosan-SWNT (S) beads under dynamic condition. a) UV-vis absorption spectra measured during MO adsorption after different periods. b) Adsorption capacities of MO by chitosan and chitosan-SWNT beads for a period of 240 min. c) UV-vis absorption spectra during Au (5 nm) adsorption after different periods. d) Adsorption capacities of Au nanoparticles (5 nm) by chitosan and chitosan-SWNT beads for a period of 3000 min. e) UV-vis absorption spectra during Au (50 nm) adsorption after different periods. f) Adsorption capacities of Au nanoparticles (50 nm) by chitosan and chitosan-SWNT beads for a period of 240 min.

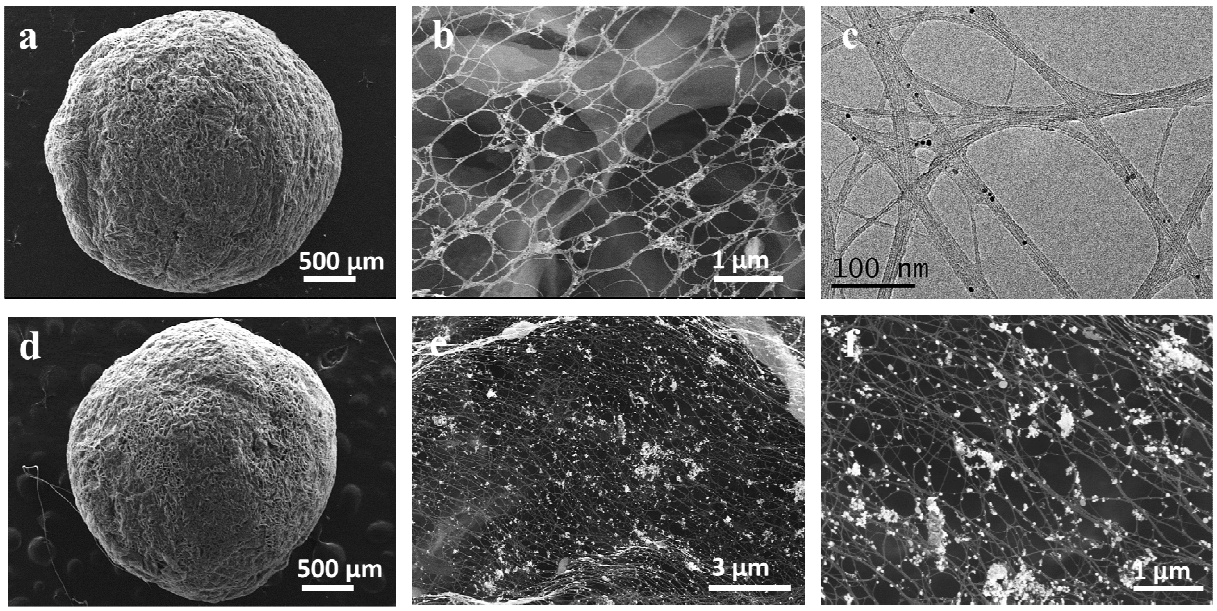

Figure 5. SEM and TEM characterization of core-shell chitosan-SWNT beads surface after adsorption of different size Au nanoparticles. a) SEM image of a chitosan-SWNT bead after adsorption of 5 nm Au nanoparticles. b) The coating SWNT film on bead surface showing 5 nm Au nanoparticles (white contrast particles) mainly adsorbed at the crossed positions. c) TEM image of the SWNT bundles with a small amount of 5 nm Au nanoparticles (the black dots) adsorbed on them. d) SEM image of a chitosan-SWNT bead after adsorption of 50 nm Au nanoparticles. e) The SWNT film with many 50 nm Au nanoparticles adhered on. f) Close view showing 50 nm Au nanoparticles attached individually to interconnected bundles or formed small aggregations within the network pores.